Supporting Information

Green and Red Phosphorescent Organic Light-Emitting Diodes with Ambipolic Hosts Based on Phenothiazine and Carbazole Moieties: Photoelectrical Properties, Morphology and Efficiency

Gintautas Bagdžiūnas[a], Gintarė Grybauskaitė[a], Nataliya Kostiv[a,b], Khrystyna Ivaniuk[b], Dmytro Volyniuk[a], Algirdas Lazauskas[c]*

[a] Department of Polymer Chemistry and Technology, Kaunas University of Technology, K. Barsausko st. 59, LT-51423, Kaunas, Lithuania.

[b] Lviv Polytechnic National University, S. Bandera 12, 79013 Lviv, Ukraine.

[c] Institute of Materials Science of Kaunas University of Technology, K. Barsausko st. 59, LT-51423 Kaunas, Lithuania.

Contents

Details of synthesis and identification

The melting points were determined in open capillaries with a digital melting point Electrothermal MEL-TEMP apparatus. All reactions and purity of the synthesized compounds were monitored by TLC using Silica gel 60 F 254 aluminum plates (Merck). ^{1}H NMR spectroscopy was carried out on a Bruker Avance 400 NMR spectrometer. The residue signals of the solvents were used as internal standards. Attenuated total reflection infrared (ATR IR) spectra were recorded using a Bruker VERTEX 70 spectrometer. MS data was recorded on UPLC-MS Acquity Waters SQ Detector 2.

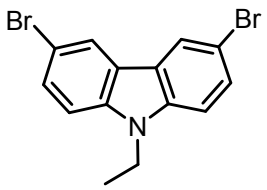

3,6-Dibromo-9-ethyl-9*H*-carbazole. 9-Ethyl-carbazole (5.00 g, 25.6 mmol) was added to a solution of N-bromosuccinimide, NBS (8.89 g, 49.9 mmol), in 50 mL of *N,N*-dimethylformamide (DMF). The reaction mixture was stirred at room temperature for 4 hours. When the reaction was completed, the solution was poured into a large amount of ice water. The yellow precipitate was filtered off and recrystallized from an izopropanol/DMF mixture to yield the product as yellowish needle-like crystals. Yield: 7.38 g (82 %), practical melting point 140-142°C, lit. melting point 141°C.[1]

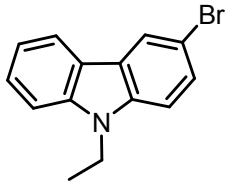

3-Bromo-9-ethyl-9*H*-carbazole. 9-Ethyl-carbazole (1.00 g, 5.12 mmol) was added to a solution of N-bromosuccinimide, NBS (0.911 g, 5.12 mmol), in 10 mL of DMF. The reaction mixture was stirred at room temperature for 24 hours. When the reaction was completed, the solution was poured into a large amount of ice water and extracted with ethyl acetate. The organic layer was dried over anhydrous sodium sulfate followed by solvent evaporation in rotary evaporator. The product was crystallized in methanol to afford the white needle-like crystals. Yield: 0.88 g (62 %), melting point 79-82°C, lit. 83°C.[2]

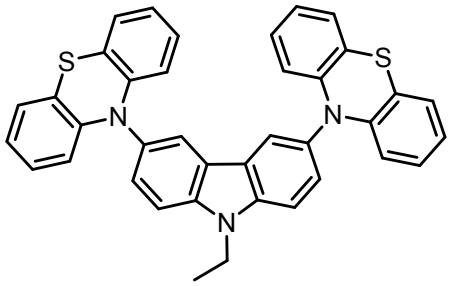

10,10‘-(9-Ethyl-9*H*-carbazole-3,6-diyl)bis(10*H*-phenothiazine (CzBisPhen). The palladium-catalyzed Buchwald-Hartwig reaction. 3,6-Dibromo-9-ethyl-9H-carbazole (0.4 g, 1.132 mmol), 10*H*-phenothiazine (0.564 g, 2.83 mmol), bis(tri-*tert*-butylphosphine)palladium(0) (0.012 g, 0.0226 mmol), potassium *tert*-butoxide (0.380 g, 3.40 mmol) dissolved in 9 ml of anhydrous toluene and refluxed 24 hours under nitrogen atmosphere at 100°C temperature. The mixture was extracted with dichloromethane and water. The organic layer was dried over anhydrous sodium sulfate followed by solvent evaporation in rotary evaporator. The product was crystallized in izopropanol/DMF mixture. Yield: 0.52 g (78%), melting point 278-280°C.

^{1}H NMR (400 MHz, d_6-DMSO) δ 8.38 (d, J = 2.0 Hz, 2H), 7.98 (d, J = 8.6 Hz, 2H), 7.53 (dd, J = 8.6, 2.1 Hz, 2H), 7.04 (dd, J = 7.4, 1.5 Hz, 4H), 6.84 (dtd, J = 21.5, 7.4, 1.5 Hz, 8H), 6.16 (dd, J = 8.1, 1.5 Hz, 4H), 4.62 (q, J = 7.0 Hz, 2H), 1.48 (t, J = 7.0 Hz, 3H).
^{13}C NMR (101 MHz, d_6-DMSO) δ 144.4, 139.5, 131.5, 128.9, 127.2, 126.5, 123.8, 123.4, 122.4, 118.5, 115.8, 111.8, 39.4, 14.0 (for DMF are 162.3, 35.7, 30.7).
IR (KBr): 3062, 2974, 1591, 1569, 1461, 1309, 1125, 1085, 1044, 814, 745, 658, 633, 613.

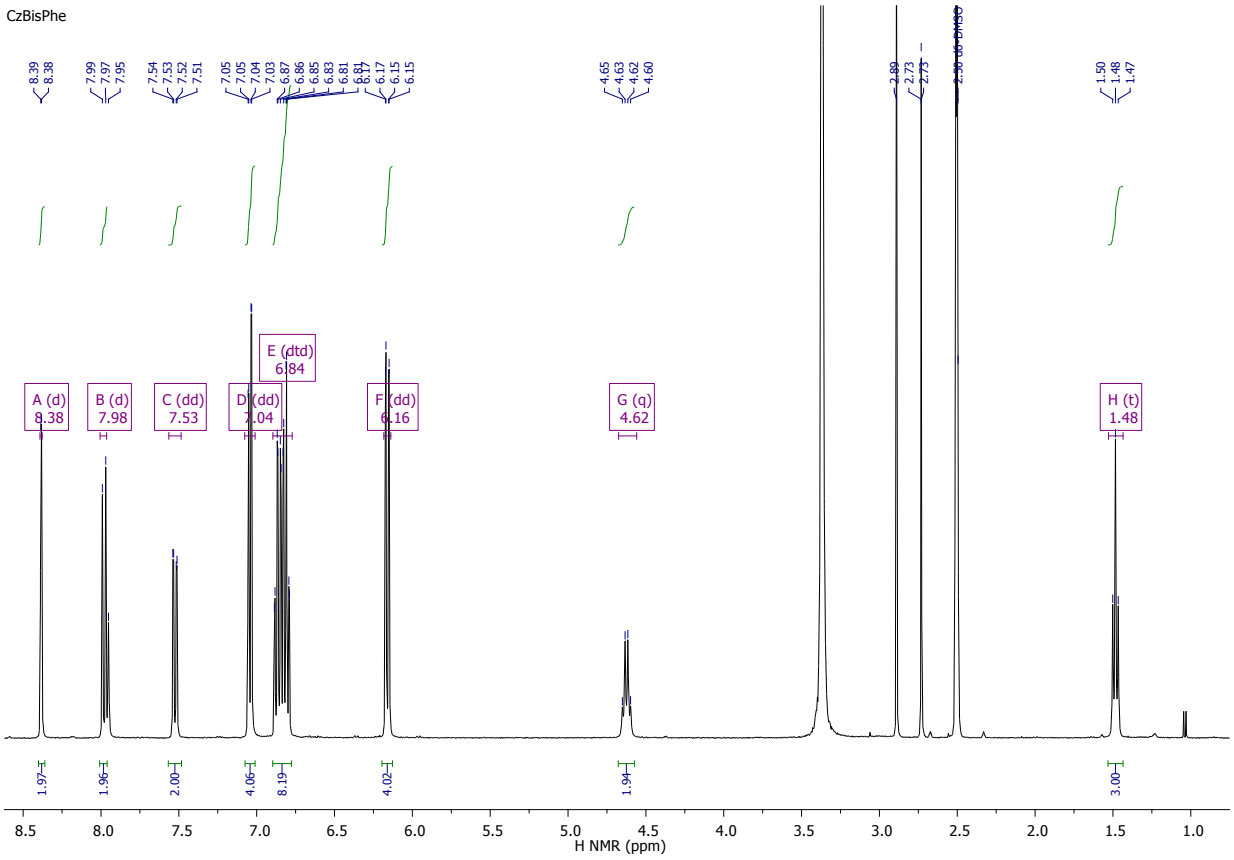
CzBisPhe
A (d) 8.38
B (d) 7.98
C (dd) 7.53
D (dd) 7.04
E (dtd) 6.84
F (dd) 6.16
G (q) 4.62
H (t) 1.48
1.97
1.96
2.00
4.06
8.19
4.02
1.94
3.00
H NMR (ppm)

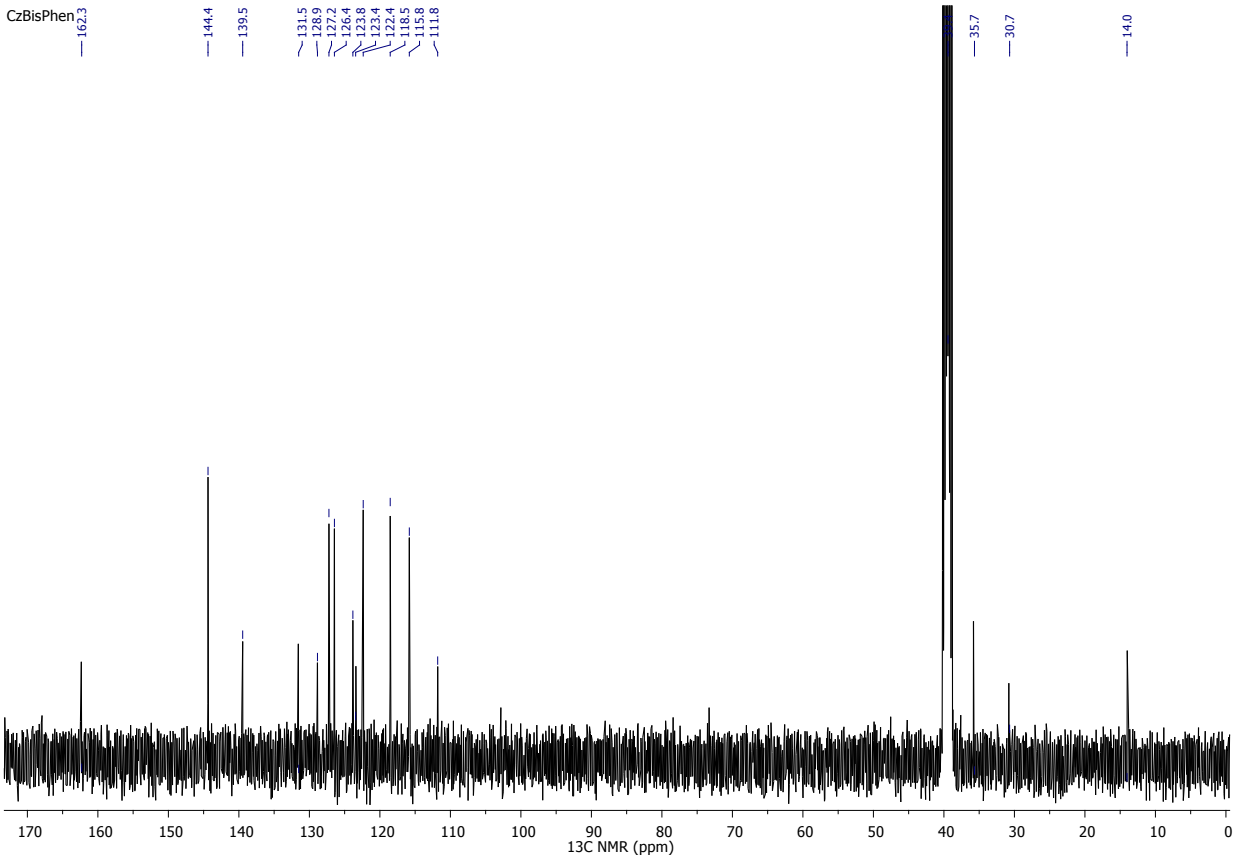
CzBisPhen
162.3
144.4
139.5
131.5
128.9
127.2
126.4
123.8
123.4
122.4
118.5
115.8
111.8
35.7
30.7
14.0
13C NMR (ppm)

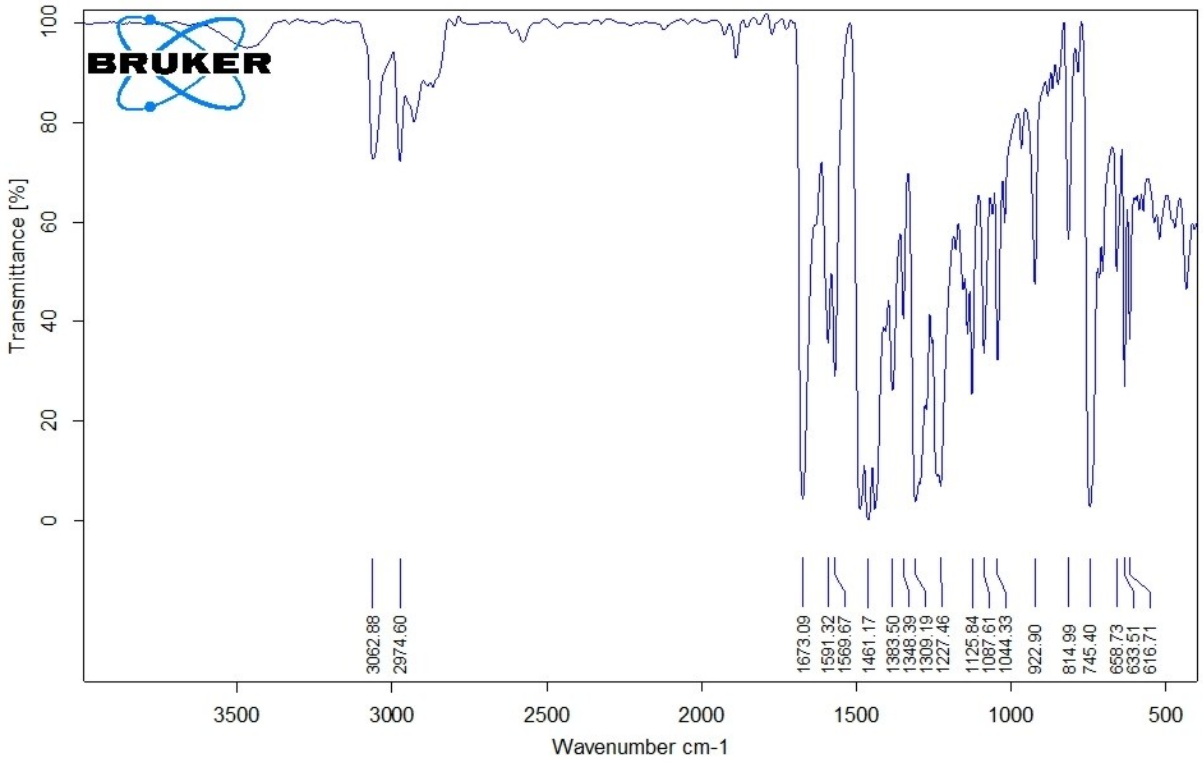
BRUKER
Transmittance [%]
Wavenumber cm-1
3062.88
2974.60
1673.09
1591.32
1569.67
1461.17
1383.50
1348.39
1309.19
1227.46
1125.84
1057.61
1044.33
922.90
814.99
745.40
658.73
633.51
616.71

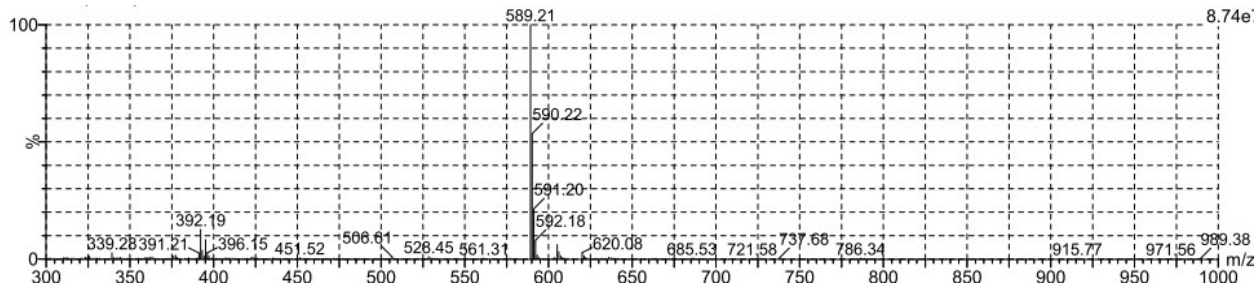

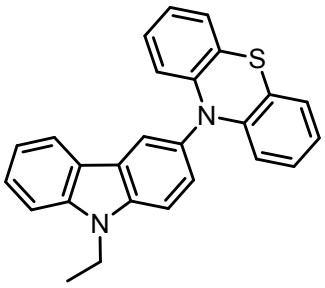

10-(9-Ethyl-9*H*-carbazol-3-yl)-10*H*-phenothiazine (CzMonoPhen). It was carried out the palladium-catalyzed Buchwald-Hartwig reaction. 3-Bromo-9-ethyl-9H-carbazole (0.4 g, 1.46 mmol), 10*H*-phenothiazine (0.349 g, 1.75 mmol), bis(tri-*tert*-butylphosphine)palladium(0) (0.015 g, 0.0292 mmol), potassium *tert*-butoxide (0.245 g, 2.19 mmol) dissolved in 9 ml of anhydrous toluene and refluxed 24 hours under nitrogen atmosphere at 100°C temperature. The mixture was extracted with dichloromethane and water. The organic layer was dried over anhydrous sodium sulfate followed by solvent evaporation in rotary evaporator. The filtrate was then evaporated under vacuum and purified by column chromatography (DCM:Hex = 1:2.5). The product was crystallized in izopropanol/DMF mixture. Yield: 0.36 g (63%), melting point 218-220°C.

^{1}H NMR (400 MHz, d_6-DMSO) δ 8.27 (d, *J* = 1.7 Hz, 1H), 8.23 (d, *J* = 7.8 Hz, 1H), 7.89 (d, *J* = 8.6 Hz, 1H), 7.68 (d, *J* = 8.6 Hz, 1H), 7.54 – 7.43 (m, 2H), 7.22 (t, *J* = 7.4 Hz, 1H), 7.05 (dd, *J* = 7.4, 1.8 Hz, 2H), 6.89 – 6.77 (m, 4H), 6.15 (dd, *J* = 7.1, 1.2 Hz, 2H), 4.53 (q, *J* = 7.0 Hz, 2H), 1.40 (t, *J* = 7.0 Hz, 3H).

^{13}C NMR (101 MHz, d_6-DMSO) δ 144.6, 140.1, 138.9, 131.2, 128.1, 127.3, 126.5, 124.1, 122.6, 122.4, 122.1, 121.0, 119.2, 118.5, 115.8, 111.3, 109.5, 37.4, 13.9.

IR (KBr): 3118, 2994, 1581, 1510, 1449, 1356, 1260, 1178, 1068, 956, 822, 790, 652.

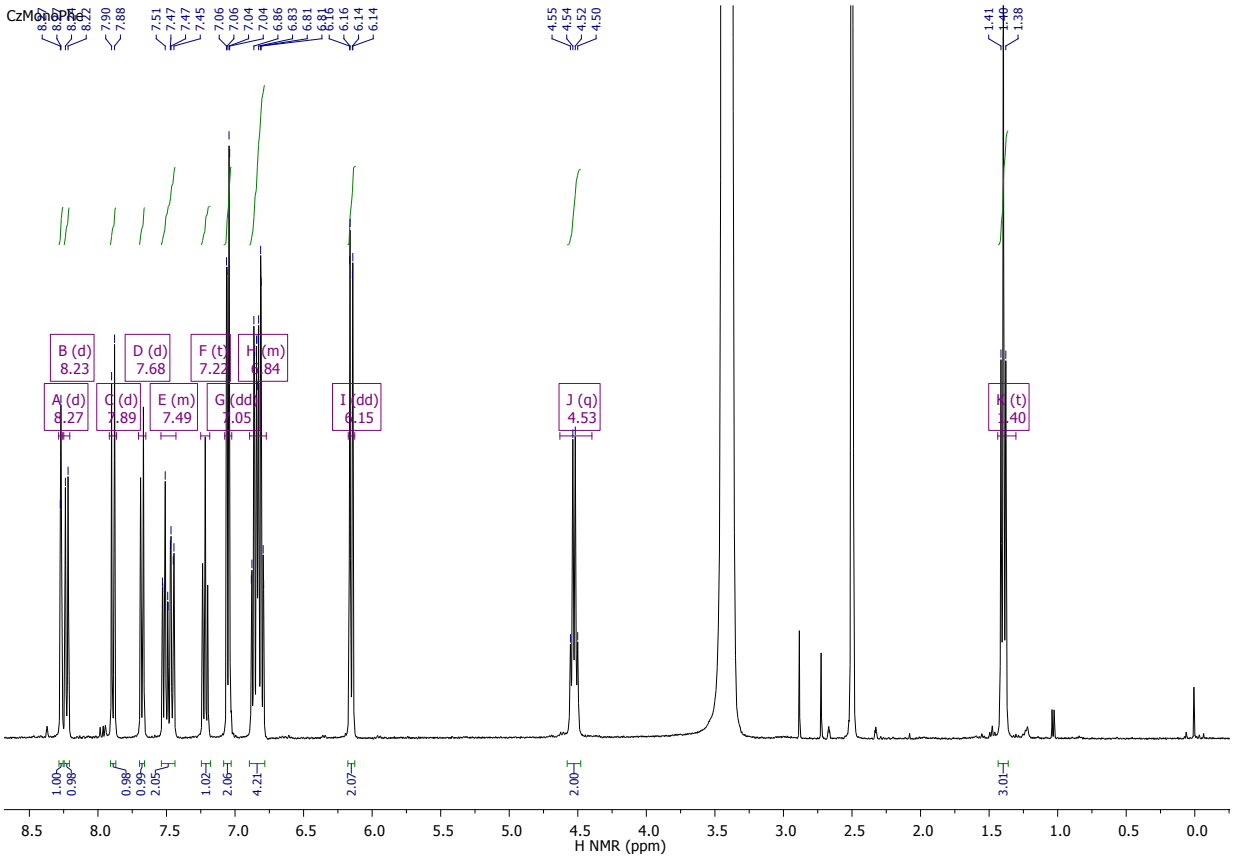
CzMonoPhe
B (d) 8.23
D (d) 7.68
A (d) 8.27
E (m) 7.49
I (dd) 6.15
J (q) 4.53
H NMR (ppm)

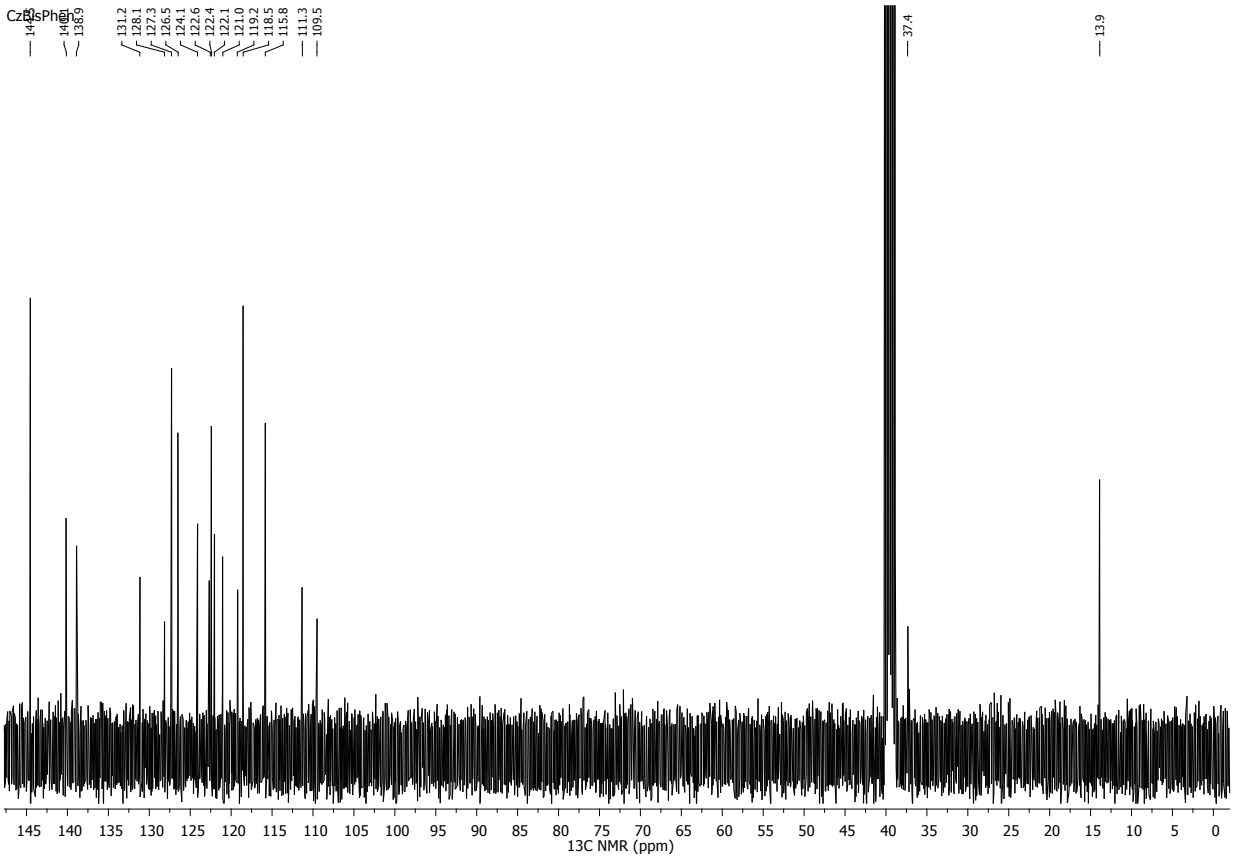
CzBisPhen
145.0
140.7
138.9
131.2
128.1
127.3
126.5
124.1
122.6
122.4
122.1
121.0
119.2
118.5
115.8
111.3
109.5
37.4
13.9
145 140 135 130 125 120 115 110 105 100 95 90 85 80 75 70 65 60 55 50 45 40 35 30 25 20 15 10 5 0
13C NMR (ppm)

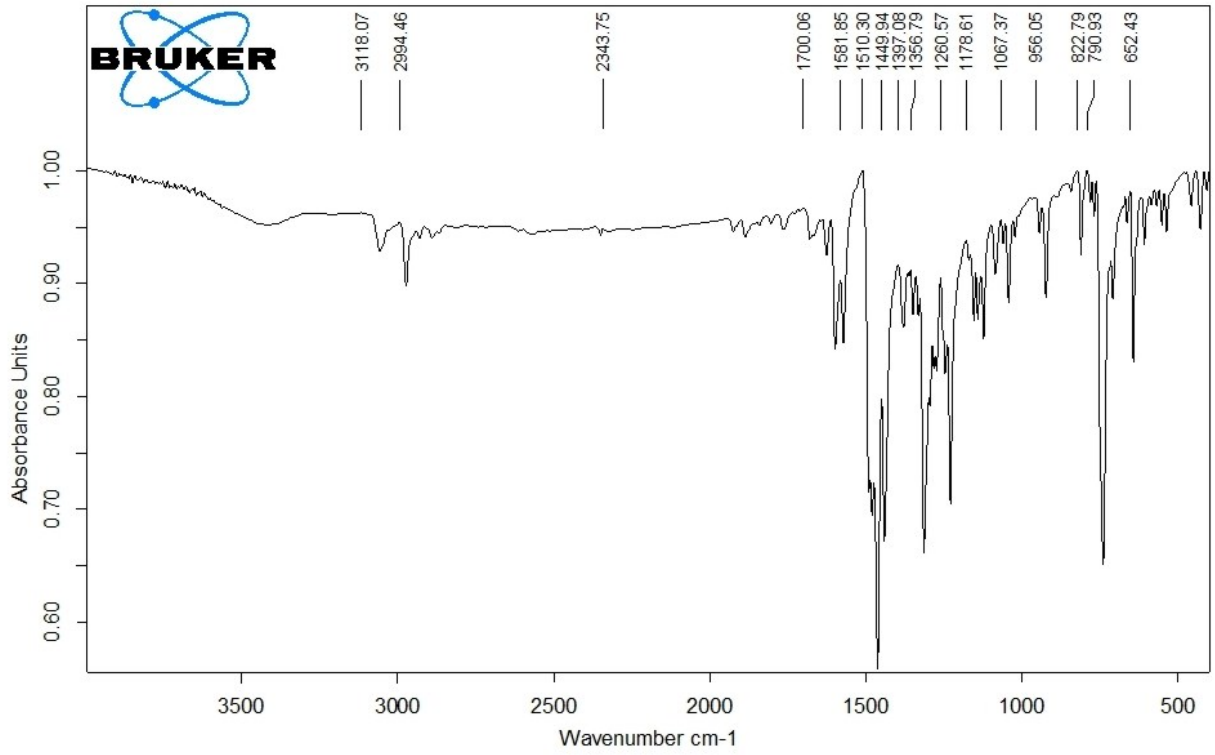
BRUKER
3118.07
2994.46
2343.75
1700.06
1581.85
1510.30
1449.94
1397.08
1356.79
1260.57
1178.61
1067.37
956.05
822.79
790.93
652.43
Absorbance Units
1.00
0.90
0.80
0.70
0.60
3500
3000
2500
2000
1500
1000
500
Wavenumber cm-1

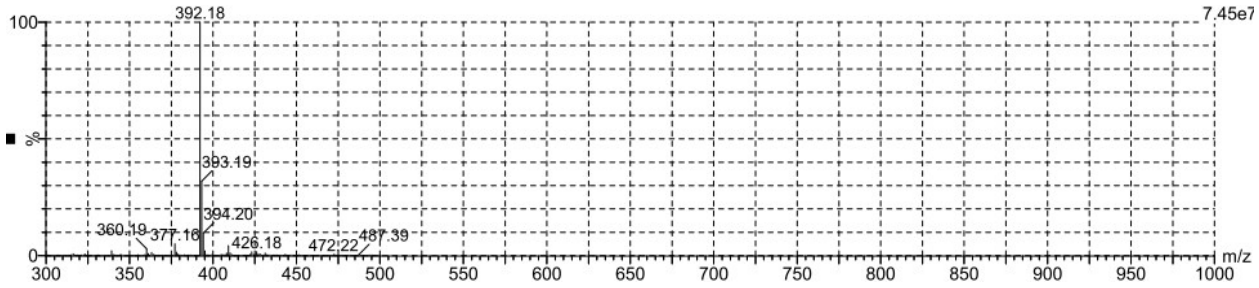

Details of X-ray diffraction measurements

The monocrystals of the **CzMonoPhen** and **CzBisPhen** compounds were obtained from the mixture of izopropanol and *N,N*-dimethylformamide. Colorless prism crystals were mounted on the glass fiber. The crystallographic analysis was performed employing XtaLAB mini diffractometer (Rigaku) with graphite monochromated Mo K_α (λ = 0.71075 Å) X-ray source. The measurements were performed at the temperature of 293 K. The crystallographic data and the crystal structures refinements are summarized in Table S1. The crystallographic data for structure reported in this paper have been deposited with Cambridge Crystallographic Data Centre as supplementary publication no CCDC 1445785-1445786 for **CzBisPhen** and **CzMonoPhen**, respectively. The copies of data can be obtained free of charge on application to CCDC.[3]

All calculations were performed using the CrystalStructure[4] crystallographic software package except for refinement, which was performed using SHELXL-97[5]. Anisotropic thermal parameters were assigned to all nonhydrogen atoms. The hydrogens were included in the structure factor calculation at idealized positions by using a riding model and refined isotropically. ORTEP structures were visualized by the Mercury 3.5.1 software.[6]

Table S1. Crystallographic and refinement data for **CzBisPhen** and **CzMonoPhen**.

Compound	**CzBisPhen**	**CzMonoPhen**
CCDC deposition numbers	1445785	1445786
Empirical formula	$C_{41}H_{34}N_4OS_2$	$C_{26}H_{20}N_2S$
Crystal dimensions (mm)	0.220 x 0.140 x 0.060	0.400 x 0.130 x 0.120
Crystal System	triclinic	triclinic
Space group	P-1 (#2)	P-1 (#2)
Z value	4	2

Unit cell lengths (Å)	a = 14.27(2) b = 15.76(2) c = 19.57(2)	a = 9.511(11) b = 10.365(10) c = 11.71(2)
Unit cell angles (deg)	α = 64.33(5) β = 68.53(5) γ = 71.15(5)	α = 75.35(4) β = 88.08(5) γ = 64.40(4)
Cell volume ($Å^3$)	3619(7)	1003(2)
Density (g/cm^3)	1.216	1.299
R-factor[a]	0.1040	0.0653
Temperature (K)	293	293

a- $R1 = \Sigma||Fo| - |Fc||/\Sigma|Fo|$

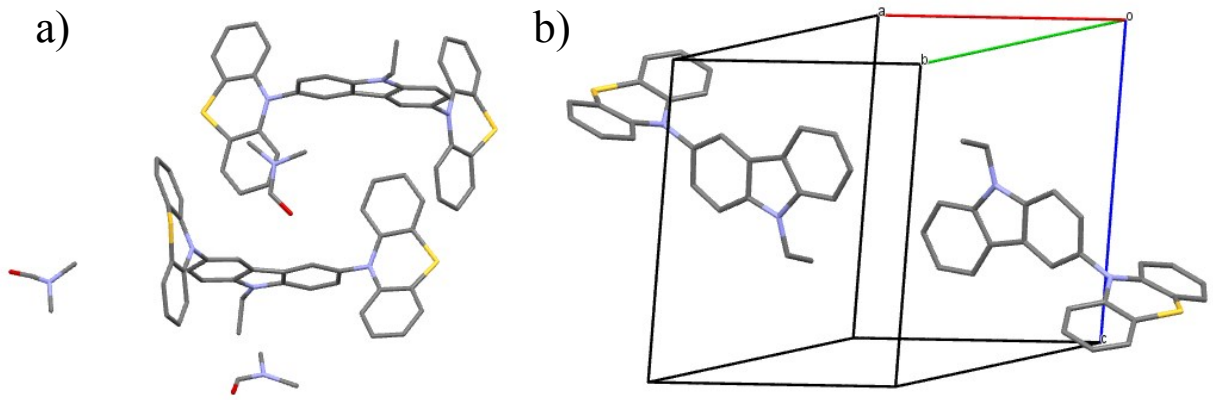

Figure S1. Asymmetric unit of crystal cell **CzBisPhen** and packing cell of **CzMonoPhen** (H atoms were removed for clarity).

The X-ray diffraction measurements at grazing incidence (XRDGI) were performed using a D8 Discover diffractometer (Bruker) with Cu K_α (λ= 1.54 Å) X-ray source. Parallel beam geometry with 60 mm Göbel mirror (X-ray mirror on a high precision parabolic surface) was used. This configuration enables transforming the divergent incident X-ray beam from a line focus of the X-ray tube into a parallel beam that is free of K_β radiation. Primary side also had a Soller slit with an axial divergence of 2.5º. The secondary side had a LYNXEYE (0D mode) detector with an opening angle of 1.275º and slit opening of 9.5 mm. Sample stage was a Centric Eulerian cradle mounted to horizontal D8 Discover with a vacuum chuck (sample holder) fixed on the top of the stage. X-ray generator voltage and current was 40.0kV and 40mA, respectively. The XRDGI

scans of the **CzMonoPhen**:Ir(ppy)$_3$, **CzBisPhen**:Ir(ppy)$_3$, **CzMonoPhen**:Ir(piq)$_2$(acac) and **CzBisPhen**:Ir(piq)$_2$(acac) layers of the mixtures deposited on the glass coverslips (Menzel Gläser) were performed in the range of 3.5-135.0º with a step size of 0.033º, time per step of 0.30 s and auto-repeat function enabled. Processing of the resultant diffractograms was performed with DIFFRAC.EVA software.

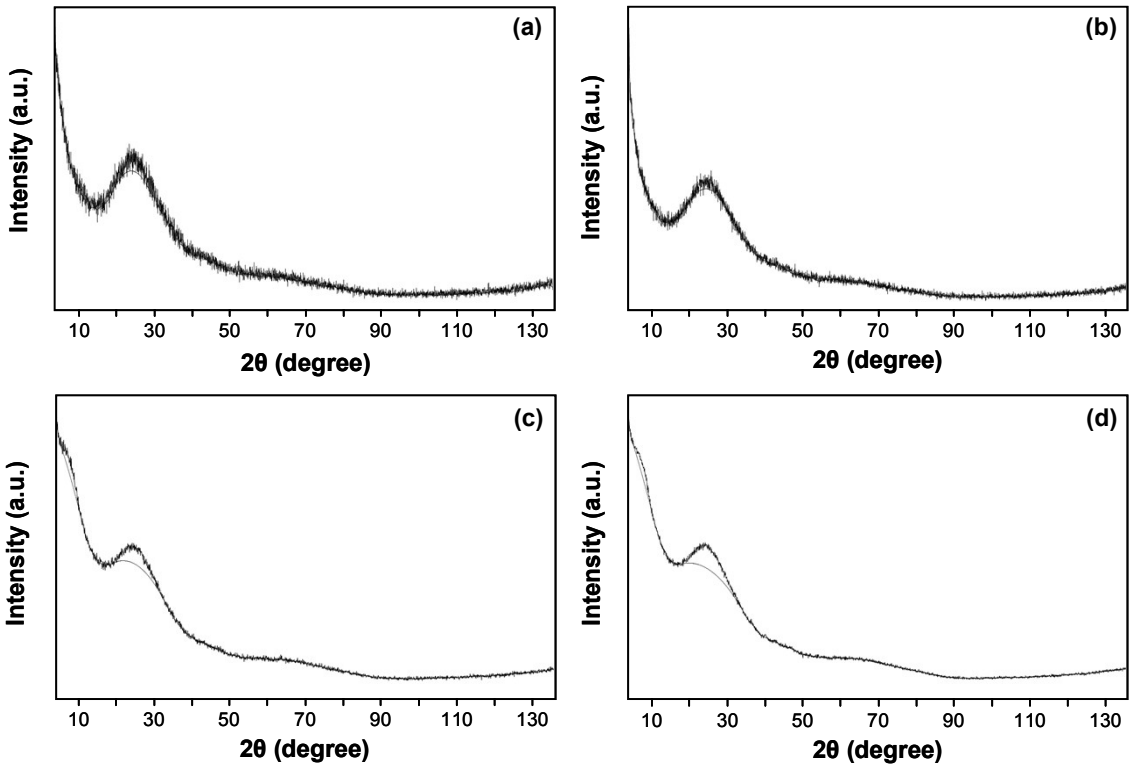

Figure S2. X-ray diffraction patterns at 1.50º grazing incidence angle of (a) **CzBisPhen**:Ir(ppy)$_3$ and (b) **CzMonoPhen**:Ir(ppy)$_3$, (c) **CzBisPhen**:Ir(piq)$_2$(acac) and (d) **CzMonoPhen**:Ir(piq)$_2$(acac) layers of mixtures.

Details of DSC and TGA analysis

Thermogravimetric analysis (TGA) was performed on the Metter TGA/SDTA851e/LF/1100 apparatus at a heating rate of 20°C/min under nitrogen atmosphere. The differential scanning calorimetry (DSC) measurements were done on a DSC Q 100 TA Instrument at a heating rate of 10°C/min under nitrogen atmosphere.

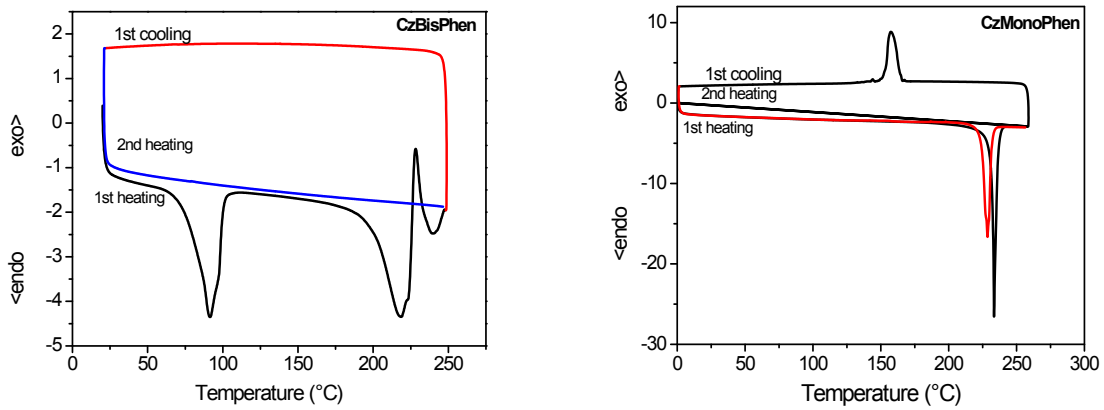

Figure S3. DSC traces of compounds: **CzBisPhen** and **CzMonoPhen**.

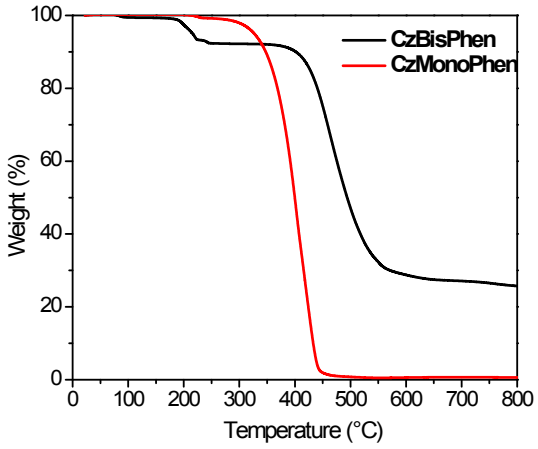

Figure S4. TGA traces of the compounds **CzBisPhen** and **CzMonoPhen**.

Details of the DFT calculations

The geometries of **CzBisPhen** and **CzMonoPhen** were optimized by the B3LYP functional and 6-31G(d,p) basis set in vacuum followed by calculations of their harmonic vibrational frequencies to verify their stability. All the calculated vibrational frequencies are real, which indicates the true minimum of total energy on a potential energy hypersurface. The rotation probability of phenothiazine moiety and single point energy of **CzBisPhen** and **CzMonoPhen** were analyzed via the theoretical potential energy scan experiment using the same level of theory, the steps of rotation of 30° were used. The intermolecular interaction energies between the molecules **CzBisPhen** and **CzMonoPhen** in dimmers were estimated using the basis set superposition effect (BSSE) concept and at wB97X-D functional with the London dispersion

corrections and 6-31G(d,p) basis set. The dimmers of molecules from X-ray analysis were generated. Dimmer 5 of **CzBisPhen** as 1 of **CzMonoPhen** was constructed and it optimized using the wB97X-D/6-31G(d) method. The excitation energy as the singlet–singlet electronic transitions are estimated with the TD-DFT/B3LYP/6-31G(d,p) method and Polarizable Continuum Model (PCM) of THF (ε = 7.6). The half-width at 1/e of the peak maximum σ value of 0.20 eV was used. Up to 30 lowest energies of the excited states were calculated in this work. All DFT calculations were done with the Spartan'14 program.[7]

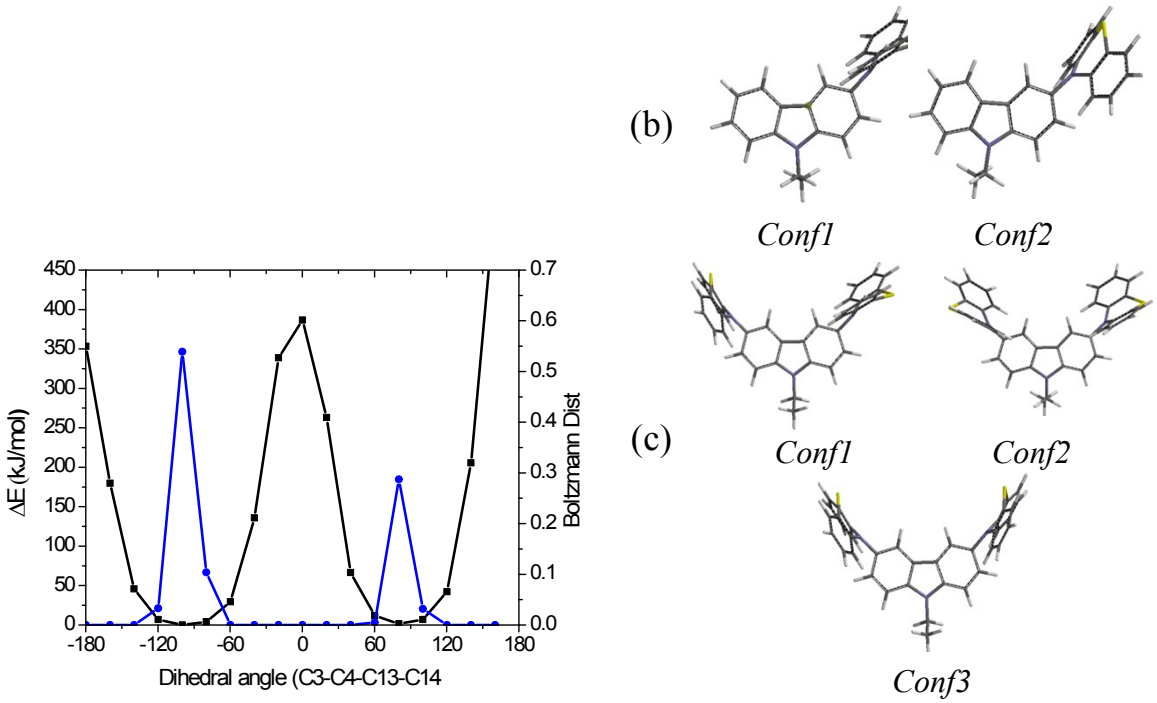

Figure S5. Potential energy scan and relative energy (black line) and Boltzmann population (blue line) of **CzMonoPhen** conformations (a) as a function of dihedral angle (C3-C4-C13-C14) at 298 K and the minimum energy conformations of **CzBisPhen** (b) and **CzMonoPhen** (c).

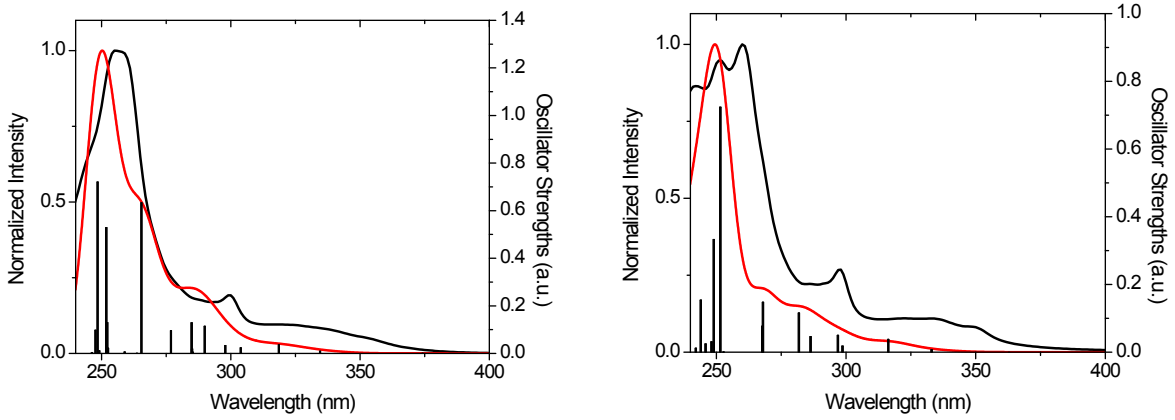

Figure S6. Comparison of the experimental (black line) and calculated UV-vis spectra of **CzBisPhen** and **CzMonoPhen** (red line) at the B3LYP/6-31G(d,p)/PCM(THF) level (σ = 0.20 eV); bars represent the oscillator strength.

Table S2. Data of the TD-DFT calculations of UV-vis spectra.

Compound	Exp. UV λ (nm)	Theor. UV λ (nm)	Electronic transition and character	Oscillator strength (*f*, au)	MO/character and contributions (%)
CzBisPhen	327	375	$S_0 \rightarrow S_1$ (CT)	0.0001	H→L (95)
		318	$S_0 \rightarrow S_5$ ($n \rightarrow \pi^*$)	0.0368	H-2→L (100)
	300	290	$S_0 \rightarrow S_{11}$ ($n \rightarrow \pi^*$)	0.1148	H→L+6 (34)
		285	$S_0 \rightarrow S_{14}$ ($\pi \rightarrow \pi^*$)	0.1292	H-3→L (45)
	256	252	$S_0 \rightarrow S_{25}$ ($\pi \rightarrow \pi^*$)	0.5292	H-2→L+3 (41)
		248	$S_0 \rightarrow S_{27}$ ($\pi \rightarrow \pi^*$)	0.7204	H-3→L+1 (45)
CzMonoPhen	330	363	$S_0 \rightarrow S_1$ (CT)	0.0001	H→L (91)
		316	$S_0 \rightarrow S_3$ ($n \rightarrow \pi^*$)	0.0379	H-1→L (94)
	297	281	$S_0 \rightarrow S_7$ ($\pi \rightarrow \pi^*$)	0.1157	H-2→L (68)
		268	$S_0 \rightarrow S_8$ ($n \rightarrow \pi^*$)	0.1478	H→L+1 (82)
	260	252	$S_0 \rightarrow S_{11}$ ($\pi \rightarrow \pi^*$)	0.7238	H-1→L+3 (59)

(a) **CzBisPhen**

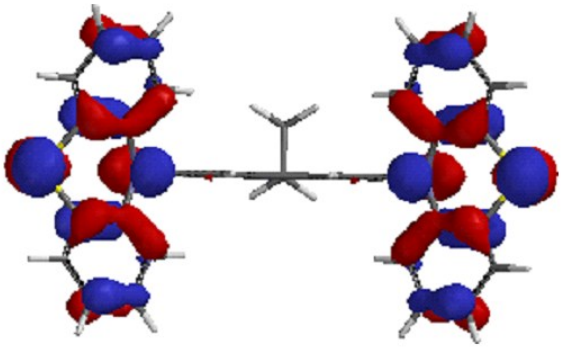

HOMO

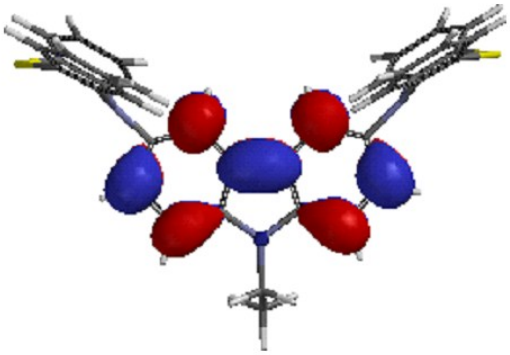

LUMO

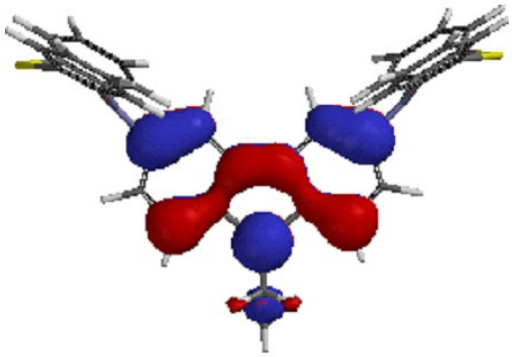

HOMO-2

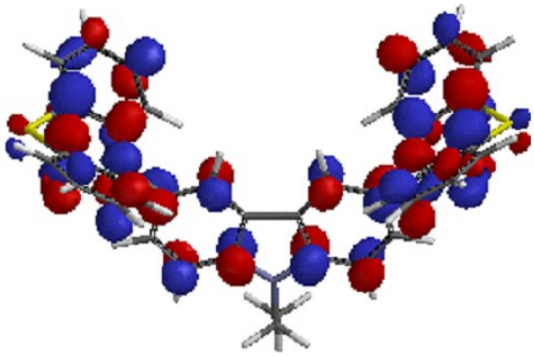

LUMO+1

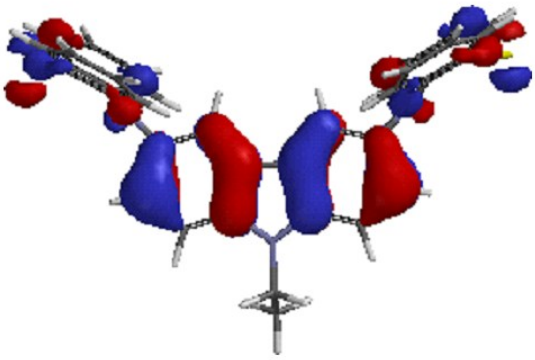

HOMO-3

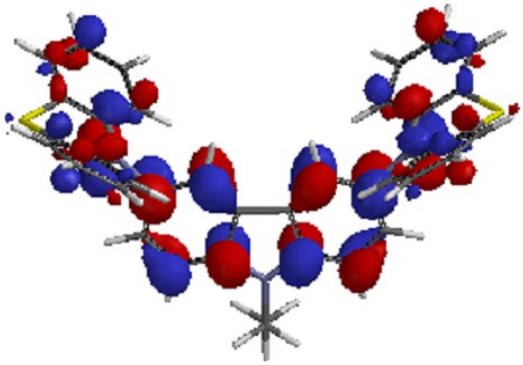

LUMO+3

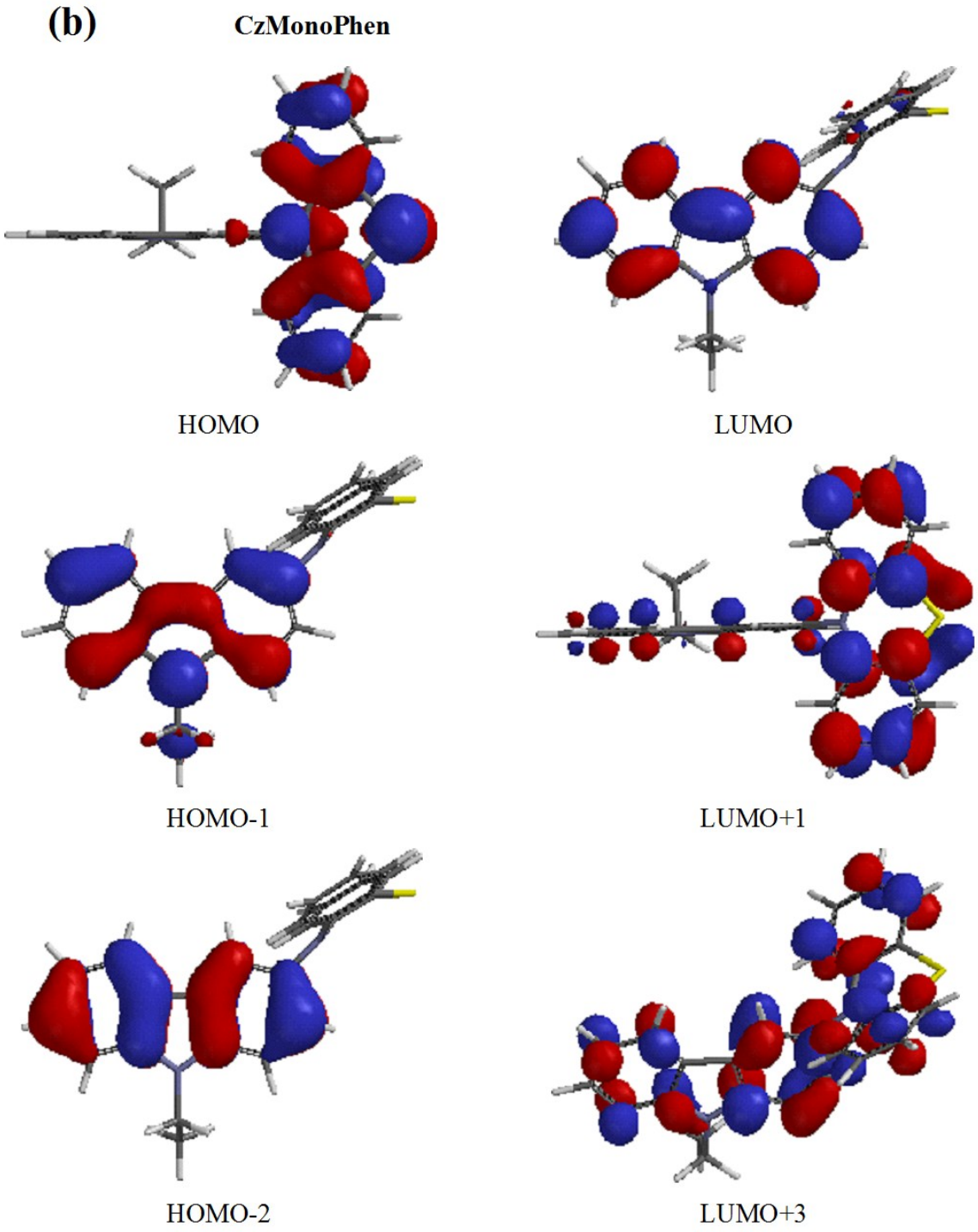

Figure S7. The computed spatial distributions of HOMO and LUMO orbitals for **CzBisPhen (a)** and **CzMonoPhen (b).**

Instrumentation for UV-vis, fluorescence, CV and electron photoemission spectroscopy

UV/Vis absorption spectra were recorded with Aventes AvaSpec-2048XL spectrometer. Photoluminescence spectra and fluorescence decay curves were recorded employing FLS980 spectrometer (Edinburgh Instruments) with TMS300 monochromator and R928P detector (Hamamatsu). The fluorescence quantum yields were measured using an integrated sphere (inside diameter of 120 mm) spherical cavity calibrated with two analytical standards: quinine sulfate in 0.1 M H_2SO_4 and rhodamine 6G in ethanol.

The cyclic voltammetry (CV) measurements were carried out with a glassy carbon electrode in a three electrode cell. The freshly distilled CaH_2 dichloromethane solutions containing 0.1 M tetrabutylammonium hexafluorophosphate (electrolyte) were used. The measurements were performed at the room temperature under argon atmosphere at 100 mV/s potential rate. The electrochemical cell included platinum wire (diameter of 1 mm) served as working electrode; Ag wire calibrated via ferrocene/ferrocinium redox couple (quasi-reference electrode) and a platinum coil (auxiliary electrode).

The electron photoemission spectra of the thin solid compound layers deposited on indium tin oxide (ITO) coated glass substrates were recorded under negative voltage of 300 V, deep UV illumination (deuterium light source ASBN-D130-CM), CM110 1/8m monochromator used and 6517B electrometer (Keithley) connected to a counter-electrode.

Details of charge mobility calculations

The time-of-flight (ToF) method was used for the estimation of hole and electron mobilities in the **CzMonoPhen** and **CzBisPhen** layers. The ToF experiments were performed on ITO/ **CzMonoPhen** and **CzBisPhen** /Al samples.The layers were deposited under the vacuum of 2-5×10^{-6} Pa. The thickness (d) of **CzMonoPhen** and **CzBisPhen** layers was 3.75 and 4.15 μm as determined via quartz resonator in PVD process, respectively. The 355 nm wavelength laser (EKSPLA NL300) excitation was used to generate the charges in the layers. Positive and negative external voltages (U) were applied to the samples to measure the hole and electron mobilities employing 6517B electrometer (Keithley). The TDS 3032C oscilloscope (Tektronix) was used to record the photocurrent transients under the different electric fields for holes and electrons transported in the **CzMonoPhen** and **CzBisPhen** layers. The charge mobilities were evaluated from the equation $\mu=d^2/(U\times t_{tr})$, where t_{tr} is a transit time. For the layer of **CzBisPhen**, both the μ_h and μ_e conform Poole–Frenkel type electric field dependence ($\mu=\mu_0\times\exp(\beta E^{1/2})$,

where μ_0 is the zero electric field charge mobility, and β is the field dependence parameter (Figures S8, table S3).[8]

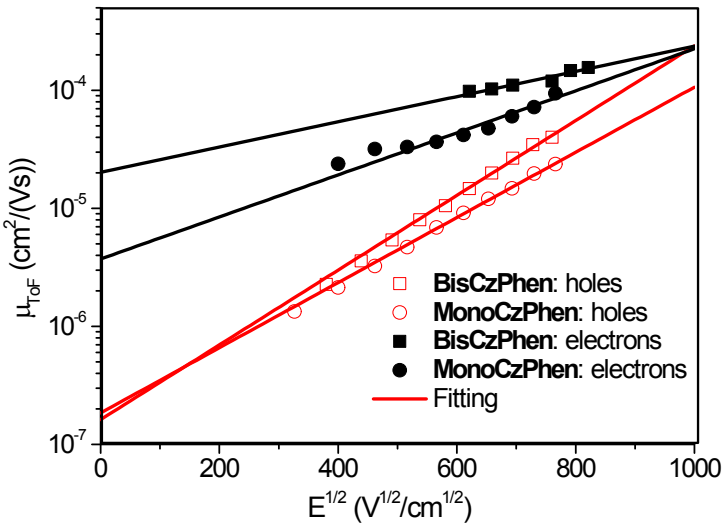

Figure S8. Electric field dependences of charge mobilities in the layers of of **CzMonoPhen** and **CzBisPhen**.

The differences in shapes of the current transients for holes and electrons for **CzMonoPhen** and **CzBisPhen** were observed (Figures S9). To estimate the current transients in terms of dispersion for charge transport, we defined a dispersion parameter from lines near the transit time using the Scher-Montroll formalism.[9] According to this formalism, the current transients can be described by the formulas:[10]

$I(t) \sim t^{-(1-\alpha_1)}$, when $t<t_{tr}$,

$I(t) \sim t^{-(1+\alpha_2)}$, when $t>t_{tr}$,

where I(t) corresponds to the two lines with slopes $(1-\alpha_1)$ (the slope prior the transit time) and $(1+\alpha_2)$ (the slope after the transit time) in a double logarithmic plot, and α is a parameter describing the dispersivity of the current transients.

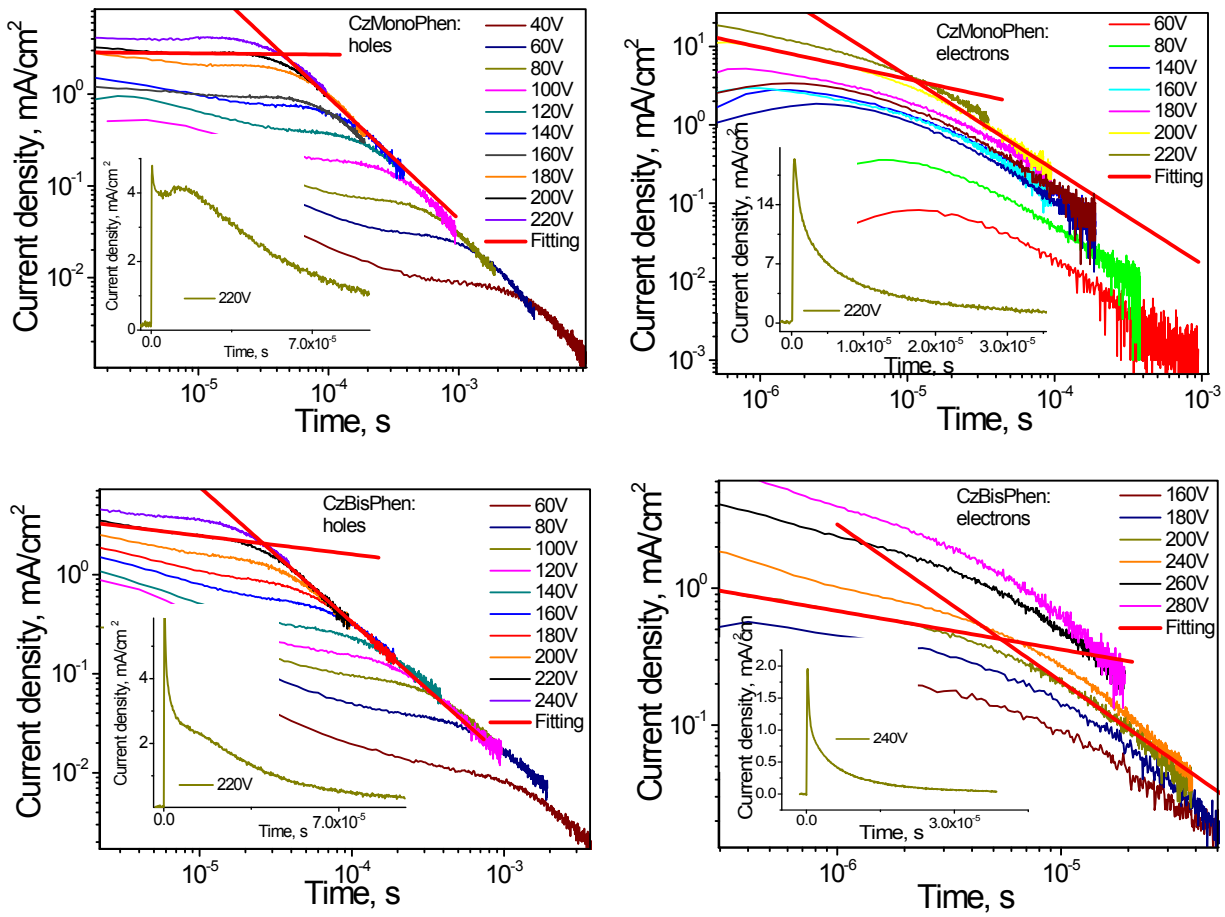

Figure S9. Holes (a,c) and electrons (b,d) ToF pulses for the layers of **CzMonoPhen** and **CzBisPhen**.

The values of the slope parameters $(1-\alpha_1)$ and $(1+\alpha_2)$ for the hole and electron transients of **CzMonoPhen** and **CzBisPhen** were determined at an electric field of ca. $5 \cdot 10^5$ V/cm at room temperature. According to the requirements of Scher-Montroll formalism, the current transients were obtained at various electric fields and the thicknesses of ToF samples were superimposed when they were normalized to the transit times. The slopes prior $(1-\alpha_1)$ and after $(1+\alpha_2)$ of the transit time have to sum up to 2.[14] Despite of the observed disagreements, the prediction is acceptable for the analysis of the shape of the current transients for evaluating the occurrence of dispersion.[15] The fitted lines (the red lines) are shown in Figure 7 and the slope parameters are summarized in Table 2. The slope parameters $(1-\alpha_1)$ for holes for the layers of **CzMonoPhen** and **CzBisPhen** were found to be close to zero which corresponded to nondispersive transients. The similar observation was reported for poly(3-hexylthioatiophene).[11] The hole transport in the vacuum deposited layers of **CzMonoPhen** and **CzBisPhen** is characterized as nondispersive

transport, however, the slope parameters $(1+\alpha_1)$ for them are far from 2, which correspond to the dispersive transients. The values of the slope parameters $(1-\alpha_1)$ and $(1+\alpha_2)$ for electron transients clearly indicated the dispersive electron transport for the studied materials.

Table S3. Charge transport parameters for **CzMonoPhen** and **CzBisPhen** (hydrogens were removed for clarity).

Compound	$\mu_{0,}$ $cm^2/(V\times s)$		$\beta,$ $(cm/V)^{0.5}$		$(1-\alpha_1)$	$(1+\alpha_2)$	$(1-\alpha_1)$	$(1+\alpha_2)$
	holes	electrons	holes	electrons	holes		electrons	
CzMonoPhen	1.85×10^{-7}	3.72×10^{-6}	0.0064	0.0041	0.13	1.33	0.4	1.2
CzBisPhen	1.62×10^{-7}	2.02×10^{-5}	0.0073	0.0025	0.19	1.36	0.28	1.15

CzBisPhen	**CzMonoPhen**
Pathway 1	Pathway 1
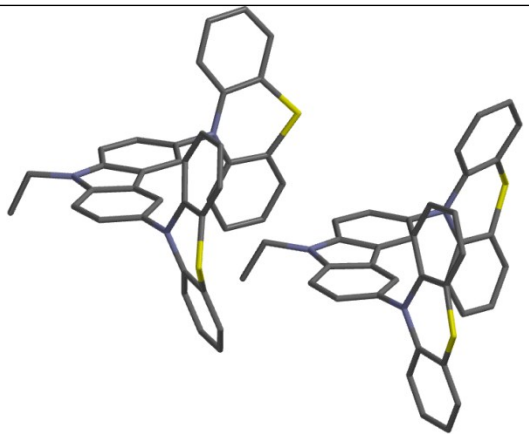	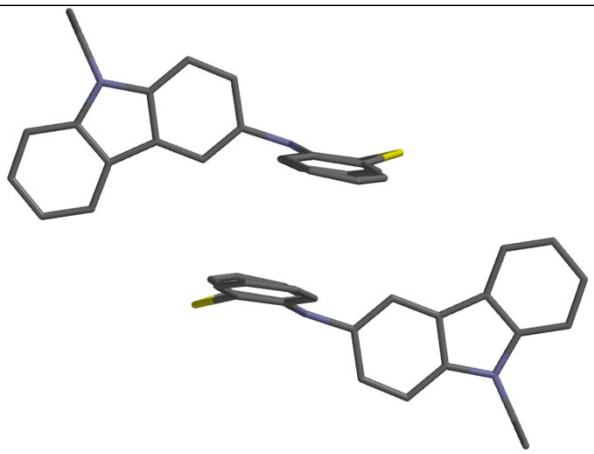
Pathway 2	Pathway 2

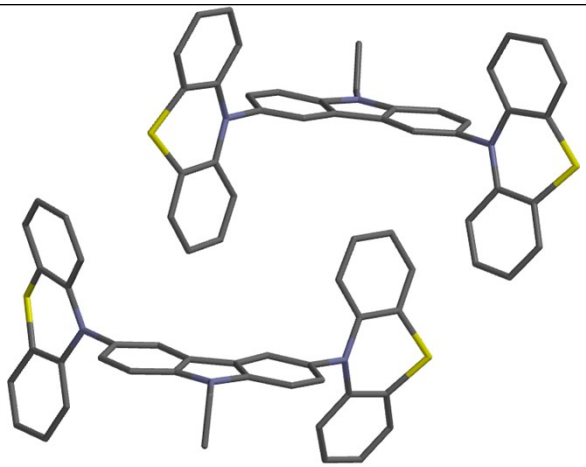	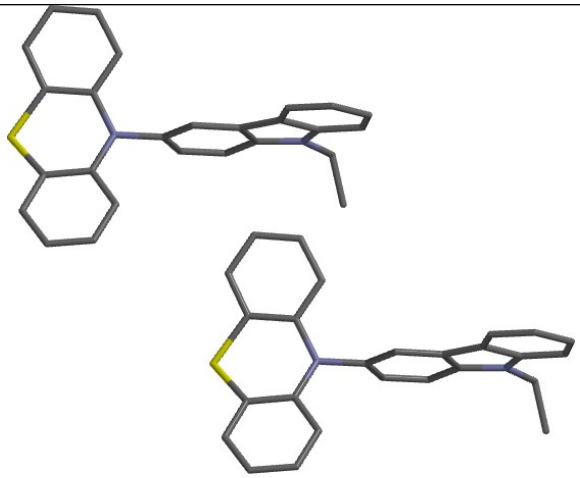
Pathway 3	Pathway 3
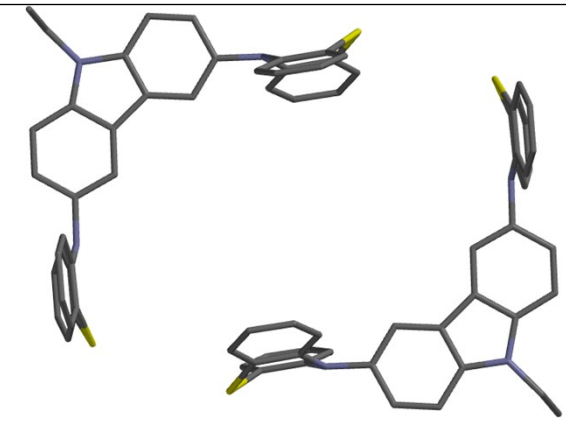	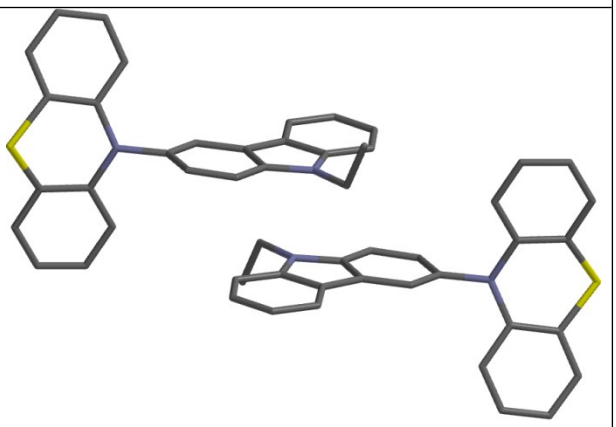
Pathway 4	Pathway 4
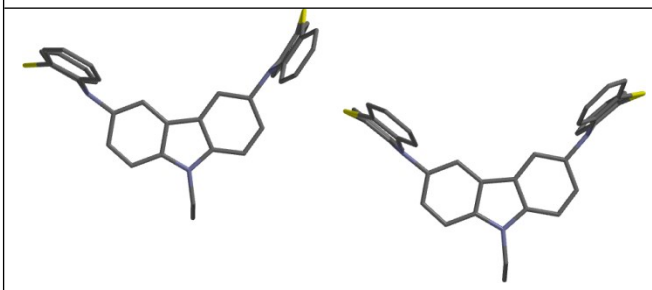	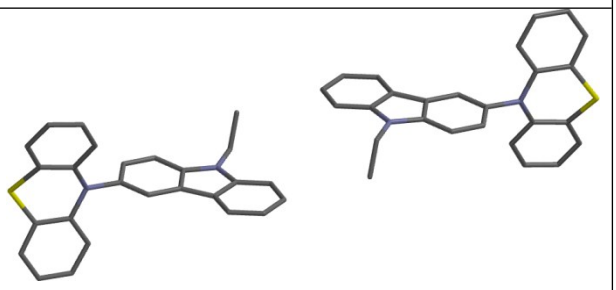
Pathway 5	Pathway 5

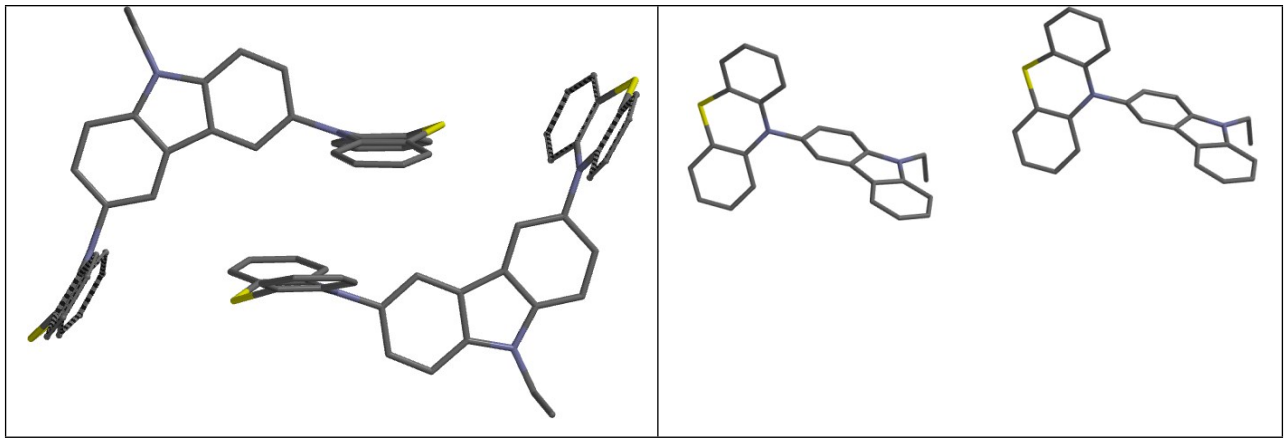

Figure S10. Possible carrier hopping pathways (dimmers) for **CzMonoPhen** and **CzBisPhen**.

Table S4. Theoretical calculation data of the hole and electron mobilities of **CzBisPhen** and **CzMonoPhen.**

CzBisPhen (λ_+ =0.38 eV, λ_- =0.26 eV)						
Pathway	d(D-D), Å	d(A-A), Å	H_h, meV	H_e, meV	E_i, kJ/mol	P_i
1	8.05	8.11	59.5	305	-46.9	3.53×10^{-3}
2	8.14	11.1	64.0	50.2	-59.9	0.670
3	7.93	16.2	0.15	0.10	-14.2	6.77×10^{-9}
4	6.82	14.1	56.5	11.4	-33.4	1.55×10^{-9}
5*	4.88	13.8	44.2	11.1	-58.0	0.317
CzMonoPhen (λ_+ =0.39 eV, λ_- =0.22 eV)						
1	4.88	10.5	44.2	11.1	-59.0	0.765
2	9.51	9.51	3.0	3.60	-26.3	1.40×10^{-6}
3	11.7	4.46	0.25	74.8	-56.1	0.235
4	17.6	7.94	0.01	29.4	-11.1	3.11×10^{-9}
5	13.5	13.5	54.9	45.6	-7.55	7.33×10^{-10}

Fabrication and characterization of PhOLEDs

PhOLEDs were fabricated employing PVD process under the vacuum higher than of $3\cdot10^{-6}$ mBar. The **CzMonoPhen**:$Ir(ppy)_3$, **CzBisPhen**:$Ir(ppy)_3$, **CzMonoPhen**:$Ir(piq)_2(acac)$, and **CzBisPhen**:$Ir(piq)_2(acac)$ host:guest emission layers were deposited by co-deposition of host (m/m 90%) and guest (m/m 10%) materials from two different sources. The deposition rates of

$Ir(piq)_2(acac)$ and $Ir(piq)_2(acac)$ were adjusted to 0.15 Å/s, while the deposition rates of **CzMonoPhen** and **CzBisPhen** were adjusted to 1.5 Å/s, respectively. The deposition rates for calcium and aluminum were kept at around 5 Å/s. The ITO with a sheet resistance of 70-100Ω/sq, was used as the anode. The current density–voltage characteristics of the devices were recorded employing 2400 series SourceMeter (Keithley). The current density–luminance characteristics were estimated using a calibrated silicon photodiode with the 6517B electrometer (Keithley). Electroluminescence (EL) spectra were recorded employing AvaSpec-2048XL spectrophotometer (Aventes). The external quantum, current and power efficiencies were calculated utilizing the luminance, current density, and EL spectra as reported earlier.[12]

Table S5. All energy levels of used materials.

Material	IP (eV)	EA (eV)	$E(T_1)$ (eV)	Ref.
mTDATA	5.1	1.9	2.65	[13]
CzBisPhen	5.25	1.55	2.61	-
CzMonoPhen	5.10	1.45	2.60	-
$Ir(ppy)_3$	5.3	2.0	2.54	[14]
$Ir(piq)_2(acac)$	5.25	2.0	2.0	[15]
Bphen	6.4	2.9	2.5	[16]

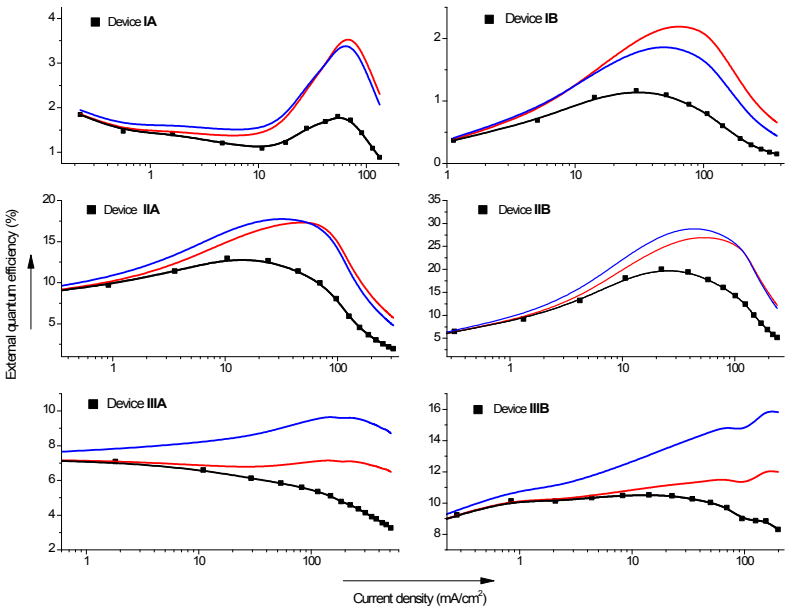

Figure S11. Measured (scatter) and fitted external quantum efficiency (black line) vs current density characteristics of **BisCzPhen** and **MonoCzPhen** containing devices. The red curves represent EQE_0 in the absence of TTA and the blue curves represent EQE_0 in the absence of TPQ.

Table S6. Data of the simulation of roll-off of PhOLEDs.

Device	Max. J_0/ mA/cm^2	Calc. J_0/ mA/cm^2	Calc. J_e/ mA/cm^2	w/ nm
IA	375	63	74	7.6
IB	375	51	97	6.1
IIA	170	110	145	13
IIB	170	146	156	17
IIIA	760	519	184	14
IIIB	760	620	243	16

Details of morphological characterization

The morphological characterization *via* AFM was performed for **CzMonoPhen**:Ir(ppy)$_3$, **CzBisPhen**:Ir(ppy)$_3$, **CzMonoPhen**:Ir(piq)$_2$(acac), and **CzBisPhen**:Ir(piq)$_2$(acac) layers of mixtures deposited on ITO/m-MTDATA (30 nm) substrates following the same deposition conditions as described for the fabrication of PhOLEDs. The AFM experiments were carried out in air at room temperature using a NanoWizardIII atomic force microscope (JPK Instruments), while data were analyzed using SurfaceXplorer and JPKSPM Data Processing software. The AFM images were collected using a V-shaped silicon cantilever (spring constant of 3 N/m, tip curvature radius of 10.0 nm and the cone angle of 20º) operating in a contact mode.

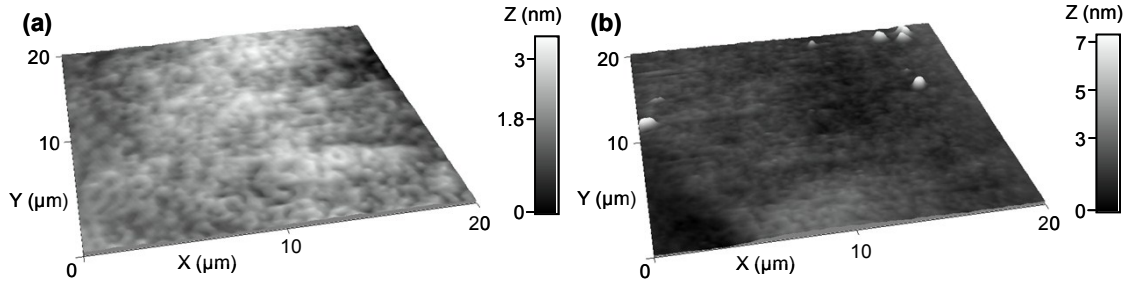

Figure S12. Characteristic AFM 3D topographical images with a normalized Z axis in nm of (a) ITO and (b) m-MTDATA layers.

Table S7. Summary of the surface morphology parameters.

Layer	Parameters		
	R_q, nm	R_{sk}	R_{ku}
ITO	0.53	-0.03	2.78
m-MTDATA	0.60	1.94	16.05
CzBisPhen:Ir(ppy)$_3$	1.62	-0.11	2.89
CzMonoPhen:Ir(ppy)$_3$	1.14	0.49	3.61
CzBisPhen:Ir(piq)$_2$(acac)	2.03	0.15	2.56
CzMonoPhen:Ir(piq)$_2$(acac)	0.48	-0.29	4.33

Atomic cartesian coordinates

The atomic cartesian coordinates of optimized by B3LYP/6-31G(d,p) structure of **CzBisPhen**

H	-0.089800	-0.410833	1.406923
C	0.314171	0.556409	1.689856
C	1.358364	3.078498	2.479941
C	0.708590	1.486272	0.723651
C	0.437827	0.886699	3.040537
C	0.957282	2.137555	3.423110
C	1.233301	2.743626	1.128000
H	1.037075	2.358036	4.482360
H	1.749135	4.040059	2.795558
C	0.708590	1.486272	-0.723651
C	0.957282	2.137555	-3.423110
C	0.314171	0.556409	-1.689856
C	1.233301	2.743626	-1.128000
C	1.358364	3.078498	-2.479941
C	0.437827	0.886699	-3.040537
H	-0.089800	-0.410833	-1.406923
H	1.749135	4.040059	-2.795558
H	1.037075	2.358036	-4.482360
N	1.562787	3.484624	0.000000
C	2.029440	4.864282	0.000000
H	2.670701	5.001186	-0.876102
H	2.670701	5.001186	0.876102
C	0.887492	5.885896	0.000000
H	0.257663	5.762859	0.885621
H	0.257663	5.762859	-0.885621
H	1.287785	6.904578	0.000000
N	0.036795	-0.029994	-4.073882
N	0.036795	-0.029994	4.073882
C	-1.340505	-0.107485	-4.412833
C	-4.076213	-0.294739	-5.101551
C	-2.336001	0.429763	-3.581139
C	-1.745996	-0.722918	-5.613889
C	-3.098828	-0.838575	-5.934835
C	-3.683952	0.348530	-3.930543
H	-2.054247	0.924881	-2.660945
H	-3.377900	-1.339422	-6.857087
H	-4.426934	0.783998	-3.268986
H	-5.125092	-0.371900	-5.369294
C	0.950399	-1.043688	-4.467364
C	2.741588	-3.080419	-5.265680
C	0.761277	-1.744611	-5.674871
C	2.067730	-1.374229	-3.683961
C	2.957427	-2.369763	-4.087805

C	1.631532	-2.768332	-6.050141
H	2.251191	-0.843896	-2.758075
H	3.817399	-2.592726	-3.463158
H	1.442643	-3.303668	-6.975916
H	3.425101	-3.864444	-5.575466
C	-1.340505	-0.107485	4.412833
C	-4.076213	-0.294739	5.101551
C	-2.336001	0.429763	3.581139
C	-1.745996	-0.722918	5.613889
C	-3.098828	-0.838575	5.934835
C	-3.683952	0.348530	3.930543
H	-2.054247	0.924881	2.660945
H	-3.377900	-1.339422	6.857087
H	-4.426934	0.783998	3.268986
H	-5.125092	-0.371900	5.369294
C	0.950399	-1.043688	4.467364
C	2.741588	-3.080419	5.265680
C	0.761277	-1.744611	5.674871
C	2.067730	-1.374229	3.683961
C	2.957427	-2.369763	4.087805
C	1.631532	-2.768332	6.050141
H	2.251191	-0.843896	2.758075
H	3.817399	-2.592726	3.463158
H	1.442643	-3.303668	6.975916
H	3.425101	-3.864444	5.575466
S	-0.524923	-1.244230	6.800793
S	-0.524923	-1.244230	-6.800793

The atomic cartesian coordinates of optimized structure by B3LYP/6-31G(d,p) of **CzMonoPhen**

H	2.488115	-0.414195	3.132305
C	3.338098	-0.385422	2.456424
C	5.571677	-0.306123	0.701701
C	3.142031	-0.265487	1.076044
C	4.636433	-0.464903	2.951211
C	5.738409	-0.424962	2.079660
C	4.265644	-0.231368	0.208447
H	4.802013	-0.557144	4.020005
H	6.743297	-0.484333	2.487227
H	6.431426	-0.270796	0.040375
C	1.969589	-0.159632	0.233846
C	0.186383	0.080389	-1.898165
C	0.595627	-0.137114	0.489903
C	2.437470	-0.065665	-1.105582
C	1.549185	0.058881	-2.178614
C	-0.294294	-0.015940	-0.579353

H	0.214314	-0.207916	1.504205
H	1.899422	0.140760	-3.202263
H	-0.535156	0.175497	-2.702769
N	3.824079	-0.126535	-1.107684
N	-1.718310	0.018287	-0.371155
C	-2.412931	-1.211716	-0.230330
C	-3.818363	-3.646996	0.060009
C	-3.813048	-1.263161	-0.380009
C	-1.736681	-2.409657	0.050185
C	-2.431111	-3.612415	0.178809
C	-4.504470	-2.462909	-0.208649
H	-0.659528	-2.401064	0.156970
H	-1.875560	-4.522651	0.384426
H	-5.585621	-2.464369	-0.310715
H	-4.363211	-4.578995	0.171786
C	-2.319319	1.249292	0.000460
C	-3.542283	3.685566	0.751813
C	-1.557724	2.321954	0.490952
C	-3.711011	1.432220	-0.125244
C	-4.312878	2.626302	0.273116
C	-2.162055	3.527273	0.848056
H	-0.484371	2.216415	0.582263
H	-5.390517	2.725923	0.183070
H	-1.541337	4.339848	1.213871
H	-4.017003	4.617885	1.040370
S	-4.704817	0.182714	-0.914993
C	4.676463	0.007857	-2.279117
H	4.148473	-0.436548	-3.128541
H	5.568703	-0.605490	-2.116885
C	5.067977	1.456610	-2.587415
H	5.707421	1.495754	-3.475127
H	5.615407	1.899668	-1.750501
H	4.181436	2.069158	-2.775189

REFERENCES

1 D. D. J. Pielichowski and J. Kyzioł, *Monatshefte für Chemie*, 1974, **105**, 1306–1312.

2 M. Bezuglyi, G. Grybauskaite, G. Bagdziunas and J. V. Grazulevicius, *Acta Crystallogr E Crystallogr Commun*, 2015, **71**, o1067–o1068.

3 The Cambridge Structural Database (CSD)- The Cambridge Crystallographic Data Centre (CCDC), (n.d.). http://www.ccdc.cam.ac.uk/solutions/csd-system/components/csd/

4 CrystalStructure 4.0: Crystal Structure Analysis Package, Rigaku Corporation (**2000-2010**). Tokyo 196-8666, Japan.

5 G. M. Sheldrick, *Acta Crystallographica Section A Foundations of Crystallography*, 2008, **64**, 112–122.

6 C. F. Macrae, I. J. Bruno, J. A. Chisholm, P. R. Edgington, P. McCabe, E. Pidcock, L. Rodriguez-Monge, R. Taylor, J. van de Streek and P. A. Wood, *Journal of Applied Crystallography*, 2008, **41**, 466–470.

7 Spartan'14 for Windows Version 1.1.2. 1840 Von Karman Avenue, Suite 370, Irvine, CA.

8 P. M. Borsenberger and J. Shi, *phys. stat. sol. (b)*, 1995, **191**, 461–469.

9 H. Scher, M.F. Shlesinger, J.T. Bendler, Time-Scale Invariance in Transport and Relaxation, Physics Today. 44 (2008) 26–34. doi:10.1063/1.881289.

10 P. M. Borsenberger, R. Richert and H. Bässler, *Phys. Rev. B*, 1993, **47**, 4289–4295.

11 A. J. Mozer, N. S. Sariciftci, A. Pivrikas, R. Österbacka, G. Juška, L. Brassat and H. Bässler, *Phys. Rev. B*, 2005, **71**, 35214.

12 S. Okamoto, K. Tanaka, Y. Izumi, H. Adachi, T. Yamaji and T. Suzuki, *Japanese Journal of Applied Physics*, 2001, **40**, L783–L784.

13 K. Goushi and C. Adachi, *Applied Physics Letters*, 2012, **101**, 23306.

14 T. Hofbeck and H. Yersin, *Inorg. Chem.*, 2010, **49**, 9290–9299.

15 C.-H. Yang, C.-C. Tai and I.-W. Sun, *J. Mater. Chem.*, 2004, **14**, 947–950.

16 J. G. Jang, H. J. Ji, J. G. Jang, H. J. Ji, *Advances in Materials Science and Engineering,* 2012, ***2012***, e192731.